Received: 15 July 2020

DOI: 10.1002/mma.7004

SPECIAL ISSUE PAPER

WILEY

Effects of local nonequilibrium in rapid eutectic solidification—Part 2: Analysis of effects and comparison to experiment

Junfeng Xu[1,2] | **Markus Rettenmayr**[1] | **Peter K. Galenko**[1,3]

[1]Otto Schott Institute of Materials Research, Friedrich-Schiller-Universität Jena, Jena, Germany

[2]School of Materials and Chemical Engineering, Xi'an Technological University, Xi'an, China

[3]Laboratory of Multi-scale Mathematical Modeling, Department of Theoretical and Mathematical Physics, Ural Federal University, Ekaterinburg, Russia

Correspondence
Peter K. Galenko, Otto Schott Institute of Materials Research, Friedrich-Schiller-Universität Jena, Jena 07743, Germany.
Email: peter.galenko@uni-jena.de

Communicated by: I. Nizovtseva

Funding information
Foundation of Shaanxi Provincial Department of Education, Grant/Award Number: 18JS050; Science and Technology Program of Shaanxi Province, Grant/Award Number: 2016KJXX-87; German Science Foundation (DFG), Grant/Award Number: GA1142/11-1

The developed model of diffusion-limited and diffusionless solidification of a eutectic alloy describes the relation "undercooling (ΔT)-velocity (V)-interlamellar spacing (λ)" for two cases. Namely, when the solidification front velocity V is smaller than the solute diffusion speed in bulk liquid V_D, $V < V_D$, the model predicts a regime of eutectic solidification similarly to known classical models. If the solidification front velocity V is higher than the diffusion speed, $V > V_D$, the solidification is mainly controlled by kinetic and thermal undercoolings. New expressions for the solute distribution coefficient and slope of the liquidus lines are supplied. The influence of the model parameters on the growth kinetics during eutectic solidification is discussed. Model predictions are compared with experimental data for the solidification of an Fe–B alloy with eutectic composition. Computational results show that the model agrees well with experimental data especially for low and high undercoolings, extending the undercooling range that can be covered by sharp interface modeling.

KEYWORDS

diffusion, eutectic growth, interface, solidification, solute

JEL CLASSIFICATION

80A22; 82C26

1 | INTRODUCTION

Numerous reports have shown that in eutectic alloys, a lamellar eutectic forms at lower undercooling, and an anomalous eutectic forms at intermediate and larger undercooling.[1-3] If the undercooling is extremely large or the growth rate extremely fast, a chemically homogeneous single phase may form upon diffusionless transformation.[4] With the development of a eutectic growth theory, the Jackson–Hunt ("JH") model successfully explained the relationship between undercooling and growth rate.[5] The Tivedi–Magnin–Kurz ("TMK") model describes the growth characteristics under

high growth rate conditions,[6] and the Li–Zhou ("LZ") model (LZ model) describes dendritic eutectic growth, which is often found for alloys in the presence of third element impurities.[7] A modified LZ model has explained the phase fractions of anomalous eutectics.[8] The models in previous studies[5-7] sequentially reveal the true mechanism of eutectic solidification under nonequilibrium conditions.[8] The predictions of these classical models get gradually closer to experimental results. However, they do not consider the limit of solute diffusion speed during eutectic growth, and they do not predict the appearance of chemically partitionless solidification that may occur under diffusionless conditions at extreme cooling rates or very high undercoolings. Therefore, in our previous study,[9] we have derived a eutectic growth model that considers the limit of solute diffusion speed and predicts chemically homogeneous single phase solidification for diffusionless phase transformations. In the present work, we investigate how this model is affected by parameter changes concerning the characteristics of the solidification process. Namely, we will continue to discuss the effects of various physical parameters on the velocity of fast eutectic growth or on interlamellar spacings. Finally, we compare the model predictions with experimental data on the solidification of an Fe–B alloy to demonstrate the reliability of the model.

2 | BASIC EQUATIONS

The model of diffusion-limited and diffusionless solidification of eutectic alloys[9] describes the relation "undercooling (ΔT)-velocity (V)-lamellar spacing (λ)" for two cases. Namely, if the solidification front velocity V is lower than the solute diffusion speed in bulk liquid V_D, $V < V_D$, the model predicts a regime of eutectic solidification similarly to known classical models. If the solidification front velocity V is higher than the diffusion speed, $V > V_D$, the solidification is mainly controlled by kinetic and thermal undercoolings. For the calculation, an equation relating to the minimum undercooling condition gives interlamellar spacing λ and growth velocity V as follows[9]:

$$V\lambda^2 = a^L/Q^L \tag{1}$$

$$a^L = 2\left(\frac{\Gamma_\alpha \sin\theta_\alpha}{m_\alpha^v f_\alpha} + \frac{\Gamma_\beta \sin\theta_\beta}{m_\beta^v f_\beta}\right) \tag{2}$$

$$Q^L = \begin{cases} \dfrac{1}{f_\alpha f_\beta}\dfrac{\Delta C_0}{D}\left(P + \lambda\dfrac{\partial P}{\partial \lambda}\right) & Case\ I \\ \dfrac{1}{f_\alpha f_\beta}\dfrac{1-k}{D}\left(P + \lambda\dfrac{\partial P}{\partial \lambda}\right) & Case\ II \end{cases} \tag{3}$$

$$P + \lambda\frac{\partial P}{\partial \lambda} = \begin{cases} \displaystyle\sum_{n=1}^{\infty} \frac{\sin^2(n\pi f_\alpha)}{(n\pi)^3}\left(\frac{p_n\left(1-V^2/V_D^2\right)}{\sqrt{1+\left[p_n\left(1-V^2/V_D^2\right)\right]^2}+1}\right)^2 \frac{p_n}{\sqrt{1+\left[p_n\left(1-V^2/V_D^2\right)\right]^2}} & \text{Case I} \\ \displaystyle\sum_{n=1}^{\infty} \frac{\sin^2(n\pi f_\alpha)}{(n\pi)^3}\left(\frac{p_n\left(1-V^2/V_D^2\right)}{\sqrt{1+\left[p_n\left(1-V^2/V_D^2\right)\right]^2}-1+2k}\right)^2 \frac{p_n}{\sqrt{1+\left[p_n\left(1-V^2/V_D^2\right)\right]^2}} & \text{Case II} \end{cases} \tag{4}$$

where Cases I and II are for a phase diagram with cigar-shaped solid/liquid phase equilibria and a phase diagram with constant, equal distribution coefficients, respectively. The relation of undercooling ΔT, minimum interlamellar spacing λ, and growth velocity V is given as follows:

$$\Delta T = \begin{cases} \Delta T_c + \Delta T_r + \Delta T_k + \Delta T_t = m^v\left[\left(Q_0^L\lambda + \dfrac{1}{\mu}\right)V + \dfrac{a^L}{\lambda}\right] + \dfrac{\Delta H}{C_p} Iv(P_t), & V < V_D \\ \Delta T_k + \Delta T_t = m^v\dfrac{V}{\mu} + \dfrac{\Delta H}{C_p} Iv(P_t), & V \geq V_D \end{cases} \tag{5}$$

$$Q_0^L = \begin{cases} \dfrac{\Delta C_0}{f_\alpha f_\beta}\dfrac{P}{D} & Case\,I \\ \dfrac{1-k}{f_\alpha f_\beta}\dfrac{P}{D} & Case\,II \end{cases} \tag{6}$$

$$m^v = \frac{m_\alpha^v m_\beta^v}{m_\alpha^v + m_\beta^v} \tag{7}$$

$$\mu = \frac{m_\alpha^v m_\beta^v \mu_\alpha \mu_\beta}{m_\alpha^v \mu_\alpha + m_\beta^v \mu_\beta} \tag{8}$$

$$P = \begin{cases} \sum\limits_{n=1}^{\infty} \dfrac{\sin^2(n\pi f_\alpha)}{(n\pi)^3} \dfrac{p_n}{\sqrt{1+\left[p_n\left(1-V^2/V_D^2\right)\right]^2}+1} & \text{Case I} \\ \sum\limits_{n=1}^{\infty} \dfrac{\sin^2(n\pi f_\alpha)}{(n\pi)^3} \dfrac{p_n}{\sqrt{1+\left[p_n\left(1-V^2/V_D^2\right)\right]^2}-1+2k} & \text{Case II} \end{cases} \tag{9}$$

The definition of the parameters can be found in Xu and Galenko.[9] For a melt undercooled by ΔT, we can determine the growth velocity V and the minimum lamellar spacing λ. Under local equilibrium in the diffusion field described by parabolic equation, $V_D \to \infty$, the system of Equations 1–9 transforms to the expression ΔT-V-λ that was previously obtained in the LZ model.[7]

3 | EFFECTS OF MATERIAL PARAMETERS ON SOLIDIFICATION KINETICS

In this section, we demonstrate the effects of material parameters on the solidification kinetics. In particular, we consider the effect of bulk diffusion in the liquid phase, atomic redistribution at the interface and peculiarities of the phase diagram. When not mentioned otherwise, the equations for Case II ($k_\alpha = k_\beta = \text{const}$) are used for the calculations.

3.1 | Effect of diffusion coefficient

Figure 1 shows the V-ΔT curves calculated by different models with similar parameters: $\Delta C_\alpha/\Delta C_\beta/m_\alpha/m_\beta/C_E/T_e/ = 0.48/0.48/450/450/0.5/1400$, respectively. In the following, the dimensions of liquidus slope m, solute concentration C, and temperature T are all expressed by K at.%$^{-1}$, at.%, and K, respectively. It is straightforward to show that the calculated V-ΔT curve by the JH model with a constant diffusion coefficient D shows a n-power relationship; the values of V and ΔT are both unlimited in this theory. The shape of the V-ΔT curve by the TMK model shows an asymptotic value (Figure 1), appearing mainly due to temperature dependence of the diffusion coefficient given by $D(T) = D_0\exp(-E/RT)$ with the frequency factor D_0 (=8 × 10^{-8} m^2 s^{-1}), the activation energy for diffusion E (=50 000 J mol^{-1}), and the gas constant R. Using the same $D(T)$ in the JH model, the V-ΔT curve is similar to that of TMK model. Evidently, the diffusion coefficient D has a significant effect on the V-ΔT curves in diffusion controlled eutectic growth such that an increasing D leads to a higher growth front velocity V.

The V-ΔT curve for the LZ model is below that of the TMK and JH models, because the kinetic undercooling maintains the coupled eutectic growth range to higher undercoolings. If μ is large enough, the V-ΔT curve for LZ model may quantitatively coincide with that of the TMK model.

The V-ΔT curve of the present model may be lower or higher than those of the other models, depending on the value of the solute diffusion speed V_D (Figure 1). For a given equilibrium distribution coefficient k_e, if V_D is large enough, the V-ΔT curve of the present model is similar to that of the LZ model. In the range of low undercoolings, the

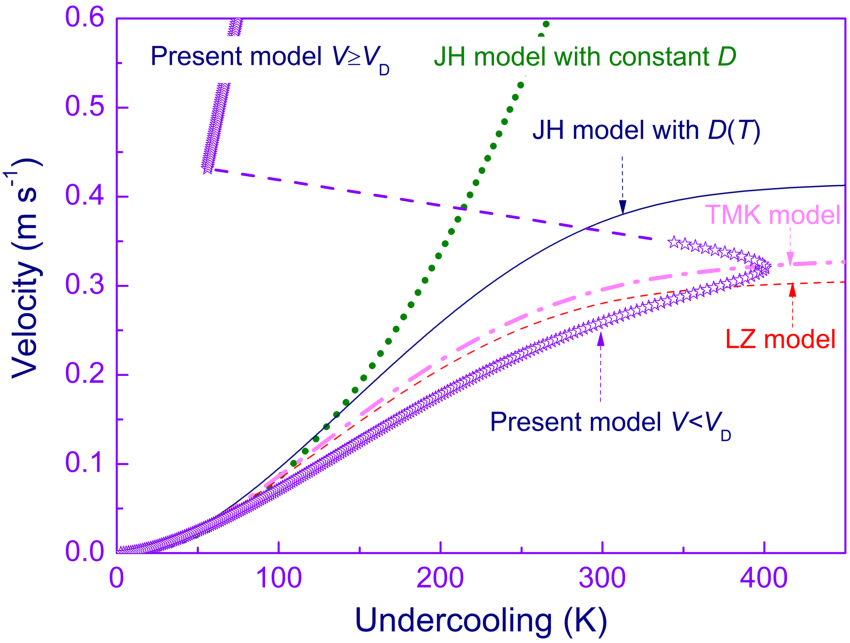

FIGURE 1 Calculated V-ΔT curves of different models employing identical material parameters [Colour figure can be viewed at wileyonlinelibrary.com]

V-ΔT curves of all models converge due to the low growth velocity in comparison with the intensity of interface and bulk diffusion processes.

3.2 | Effect of solute distribution coefficient

The solute distribution coefficient k_e reflects the difference of solid and liquid concentration at a solidifying interface. Larger values of k_e indicate that the solidus and liquidus are closer in phase diagram, which leads to higher growth velocities at a given undercooling. A low value of k_e leads to a wider solidification interval and a lower growth velocity. The JH, TMK, and LZ models assume that solute redistribution is characterized by the equilibrium partition coefficient at the interface[5-7]:

$$k_e = \frac{\text{concentration in solid}}{\text{concentration in liquid}} = \frac{C_s}{C_e} \tag{10}$$

Kurz and Trivedi[10] include the effect of solute trapping in eutectic solidification by introducing the velocity-dependent solute segregation coefficient given by Aziz.[11]

$$k(V) = \frac{k_e + V/V_{DI}}{1 + V/V_{DI}} \tag{11}$$

where V_{DI} is the diffusion speed at the interface. The quantitative analysis of the model including the function $k(V)$, Equation 11, shows a reasonable agreement with the experimental data at small and moderate growth velocities. However, experimental results indicate that complete solute trapping, that is, $k(V) = 1$, occurs at a finite interface velocity,[12] whereas Equation 11 predicts complete solute trapping only at infinite interface velocity, that is, $k(V) \to 1$ only for $V \to \infty$. To describe the increase of $k(V)$ up to $k(V) = 1$ at a finite interface velocity, both the diffusion speed at the interface V_{DI} and the diffusion speed in the bulk V_D need to be included in the model.[12] Using a generalization of Fick's law that accounts for the finite relaxation time of the diffusion flux into its steady state, one can define the solute segregation coefficient as (see Galenko and Jou[12] and references therein)

$$k(V,V_D)=\begin{cases}\dfrac{(1-V^2/{V_D}^2)\left[k_e+(1-k_e)\overline{C}_0\right]+V/V_{DI}}{1-V^2/{V_D}^2+V/V_{DI}}, & V<V_D\\ 1, \quad V\geq V_D\end{cases} \tag{12}$$

where $\overline{C}_0$ is the initial composition (in atomic fraction) for single phase growth. However, for eutectic alloys, the composition for the two solidifying phases is different, so in the steady-state regime of solidification, the solid concentration is $\overline{C}_0 = C_{s\alpha}$ for the α phase and $\overline{C}_0 = (1 - C_{s\beta})$ for the β phase.

Figure 2A shows the change of k with V predicted by Equations 10–12 using the parameters of $V_D/V_{DI}/\Delta C_\alpha/\Delta C_\beta = 2/1.6/0.48/0.48$, respectively. Then, with different expressions of k, we can further calculate V-ΔT curves for the present model, as shown in Figure 2B, where the parameters are kept constant as $\Delta C_\alpha/\Delta C_\beta/m_\alpha/m_\beta/C_E/T_e/V_D/V_{DI}/\mu_\alpha/\mu_\beta = 0.48/0.48/450/450/0.5/1400/2/1.6/0.01/0.01$, except the k values that change. It can be seen that V increases when Equations 10–12 are employed, which also shows that a larger k leads to higher velocities.

For varying $k_\alpha = k_\beta = k_e$, Figure 2C shows V-ΔT curves predicted by Equations 5 and 12. The calculation parameters are constant, particularly $m_\alpha/m_\beta/C_E/T_e/V_D/V_{DI}/\mu_\alpha/\mu_\beta = 450/450/0.5/1400/2/1.6/0.01/0.01$, respectively, only k_e changes (i.e., also ΔC_α and ΔC_β change). It can be seen that the larger k_e, the higher is the velocity. We can further calculate λ-ΔT curves with varying k_e for the present model, as shown in Figure 2D. Also in this case, a larger k_e leads to larger lamellar spacing at lower undercoolings.

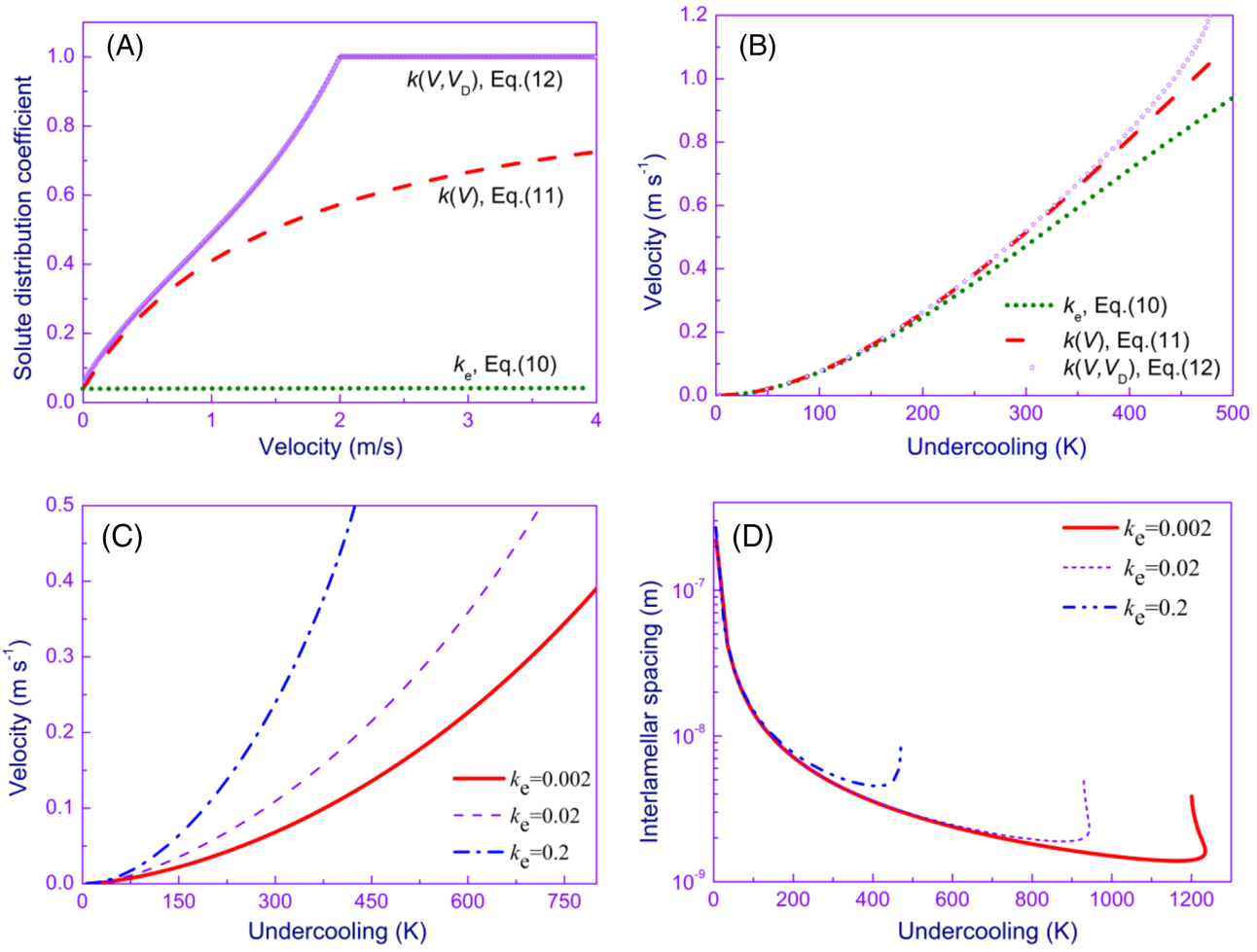

FIGURE 2 Effect of solute diffusion coefficent: (A) k as a function of V for different models (in the limit of diluted alloys, $\overline{C}_0 \rightarrow 0$ in Equation 12); (B) V-ΔT curves for different k values; (C) V-ΔT curves for different k_e values; (D) λ-ΔT curves for different k_e values [Colour figure can be viewed at wileyonlinelibrary.com]

3.3 | Effect of slope of liquidus line

The slope of the liquidus line $m = (T_m - T_e)/C_E$ describes the change of liquidus temperature with composition and the α- or β-phase melting temperature. In the JH model, the slope of the liquidus line m is directly that of the equilibrium phase diagram. In general, a change of the slope of the liquidus line in rapid solidification ("kinetic liquidus") can be described as[12]

$$m_\alpha^v = m_\alpha f(k_\alpha) \tag{13a}$$

$$m_\beta^v = m_\beta f(k_\beta) \tag{13b}$$

$$m^v = m f(k) \tag{13c}$$

$$f(k) = \frac{1-k+\ln(k/k_e)+[(1-k)(V/V_D)]^2}{1-k_e} \tag{14}$$

where m_α^v and m_β^v are the liquidus line slopes dependent on the growth velocity through the segregation coefficients k_α and k_β. In (near-) equilibrium, $V \to 0$, $k = k_e$, one gets from Equation 14: $f(k) = 1$.

Calculated with the parameters $\Delta C_\alpha/\Delta C_\beta/\mu_\alpha/\mu_\beta/C_E/T_e/V_D/k_\alpha/k_\beta = 0.48/0.48/0.01/0.01/0.5/1400/2/0.04/0.04$, respectively, Figure 3 shows the dependencies of V-ΔT_α, V-ΔT_β, and V-ΔT_I from Equations 13a, 13b, and (14) in Xu and

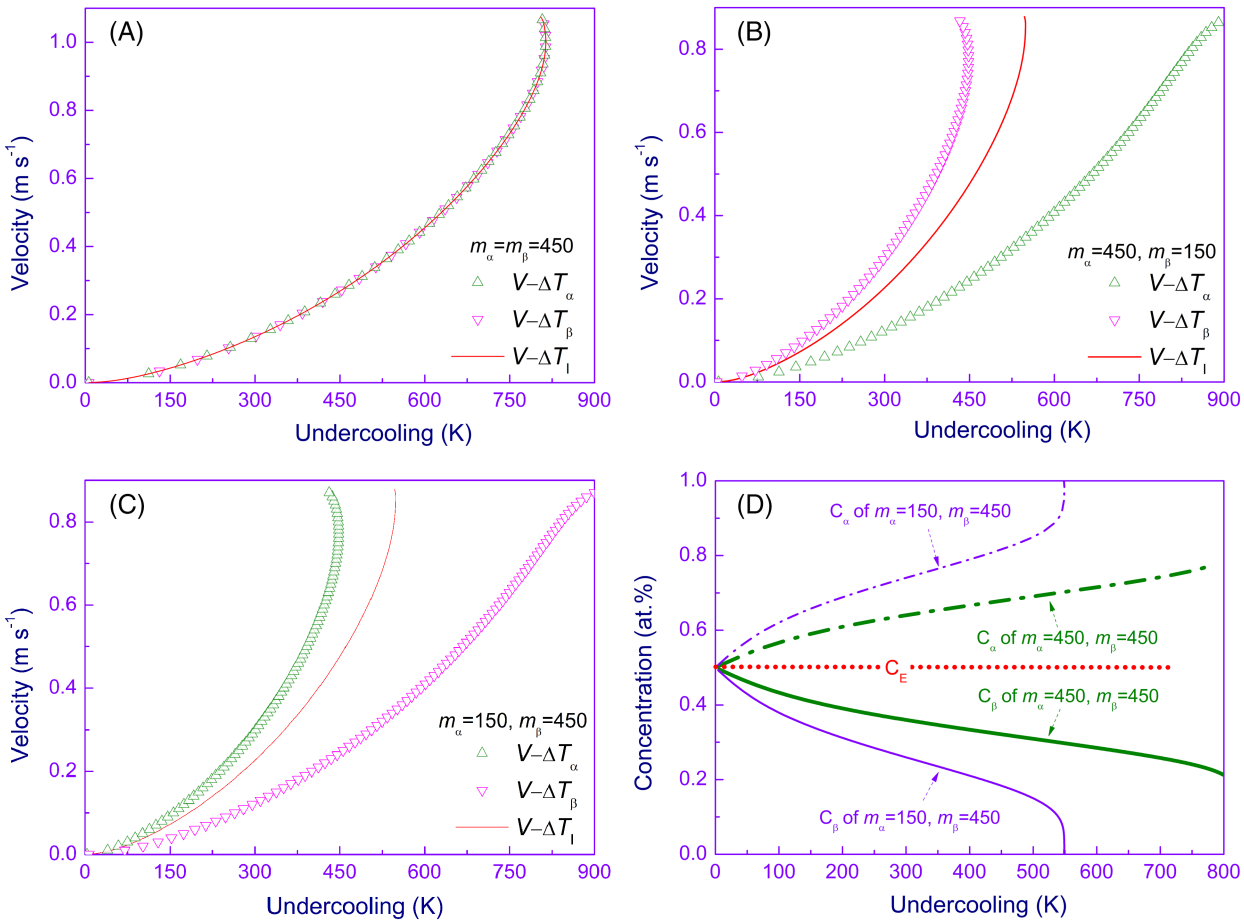

FIGURE 3 Effect of liquidus line slope: (A) $m_\alpha = m_\beta = 450$ K at.%$^{-1}$; (B) $m_\alpha = 450$ K at.%$^{-1}$, $m_\beta = 150$ K at.%$^{-1}$; (C) $m_\alpha = 150$ K at.%$^{-1}$, $m_\beta = 450$ K at.%$^{-1}$; (D) mean concentrations of the two phase interfaces for different m_α and m_β [Colour figure can be viewed at wileyonlinelibrary.com]

Galenko,[9] respectively, using varying values of m_α and m_β. With the same parameters, if $m_\alpha = m_\beta = 450$ K at.%$^{-1}$, the velocity of each phase is the same as that of coupled growth defined by V-ΔT_I (Figure 3A). For $m_\beta = 150$ K at.%$^{-1}$ and $m_\alpha = 450$ K at.%$^{-1}$, the V-ΔT_β curve is higher than the V-ΔT_I curves (Figure 3B). If we swap values of m_α and m_β, the relative positions of the V-ΔT_α and V-ΔT_β curves are changed (Figure 3C). This confirms that an increase in the liquidus slope reduces the growth velocity.

Figure 3D shows the mean solute concentrations from Equation (9) in Xu and Galenko[9] at the α- and β-phase interfaces for the cases of $m_\alpha/m_\beta = 450/450$ and $m_\alpha/m_\beta = 150/450$, respectively. It is found that when m_α changes from 450 to 150 K at.%$^{-1}$, the solute concentration at the α-phase interface C_α increases, while that for β-phase interface C_β decreases. This indicates that the lower the slope of the liquidus line, the higher is the solute concentration at the interface. It is also found that with increasing undercooling, the deviation of the solute concentrations from the eutectic composition (C_E) increases, which can be regarded as an increase of the off-equilibrium degree.

3.4 | Effect of V_D on V-ΔT and λ-ΔT curves

V_D is the critical velocity for the transition of the eutectic reaction from diffusion-limited to diffusionless. Figure 4A shows the V-ΔT curves for different V_D. The calculation parameters are $\Delta C_\alpha/\Delta C_\beta/m_\alpha/m_\beta/C_E/T_e/k_\alpha/k_\beta/\mu_\alpha/\mu_\beta = 0.48/0.48/450/450/0.5/1400/0.04/0.04/0.01/0.01$, respectively. It is found that V_D mainly affects the maximal undercooling and growth velocity. Figure 4B shows λ-ΔT curves in which the value of V_D mainly affects the maximal undercooling and minimum lamellar spacing, but it has a small effect at low undercoolings. When the undercooling is high enough, λ increases suddenly (Figure 4B). This is due to the lower diffusion coefficient D. When $V \to V_D$, the lamellar eutectic growth is gradually suppressed in such case.

3.5 | Effect of μ interface-attachment kinetics

The kinetic term $\Delta T_k = V/\mu$ is strongly dependent on the value of the kinetic coefficient μ which describes the (random) attachment of atoms under thermal activation onto the interface. Figure 5A shows V-ΔT curves for different μ values. The calculation parameters are $\Delta C_\alpha/\Delta C_\beta/m_\alpha/m_\beta/C_E/T_e/V_D/k_\alpha/k_\beta = 0.48/0.48/450/450/0.5/1400/2/0.04/0.04$, respectively. It is found that a larger μ leads to a higher growth velocity at a given undercooling. Figure 5B shows λ-ΔT curves for different μ values; μ has a negligible effect on the lamellar spacing except near the maximal undercooling. Since the kinetic undercooling is a part of the total undercooling, the kinetic effect maintains eutectic growth at a higher undercooling.

3.6 | Effect of Péclet number Pe

The function P in the JH model is described by Equation 15; it is affected by the phase fraction $f(=f\alpha)$.[5] The P-function for the TMK model is given by Equations 16a and 16b for two-type phase diagrams, where $p_n = 2n\pi/Pe$ with the

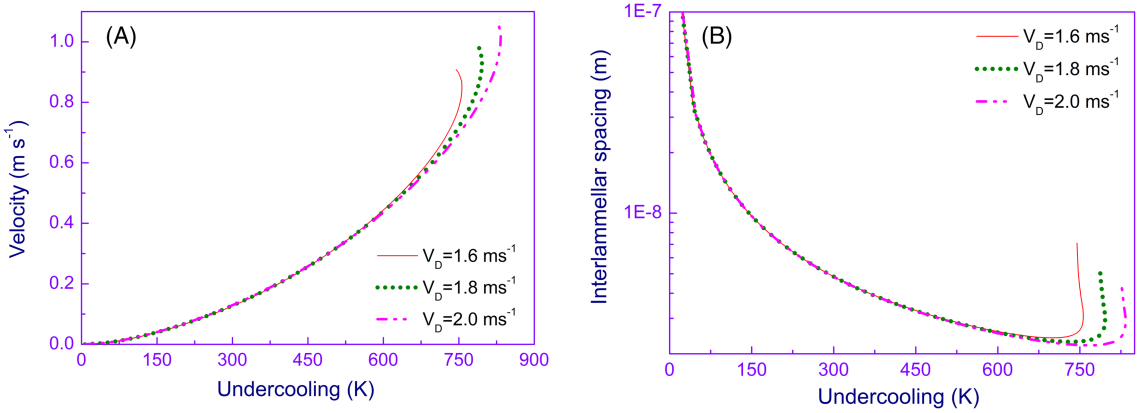

FIGURE 4 Effect of V_D on the growth velocity: (A) V-ΔT; (B) λ-ΔT [Colour figure can be viewed at wileyonlinelibrary.com]

eutectic Péclet number $Pe = V\lambda/(2D)$.[6] It changes with f, Pe, and k. For $f = 0.4$, the curves with different k are shown in Figure 6A. If $k \to 1$, the curve given by Equation 16b approaches the curve given by Equation 16a.

$$JH-model: P = \sum_{n=1}^{\infty} \frac{\sin^2(n\pi f)}{(n\pi)^3} \tag{15}$$

$$\text{Case I of TMK}-\text{model}: P = \sum_{n=1}^{\infty} \frac{sin^2(n\pi f)}{(n\pi)^3} \frac{p_n}{1+\sqrt{1+{p_n}^2}} \tag{16a}$$

$$Case\ II\ of\ TMK-model: P = \sum_{n=1}^{\infty} \frac{\sin^2(n\pi f)}{(n\pi)^3} \cdot \frac{p_n}{2k-1+\sqrt{1+{p_n}^2}} \tag{16b}$$

For the present model, P as given in Equation 9 is used. It is affected by f, k, Pe, and V_D. For constant f, k, and V_D, the value of P also increases with Pe as shown in Figure 6B, where the parameters are $f/V_D = 0.4/2$, respectively. When $k \to 1$, the kinetic curve given by Equation 9 Case II ($k_\alpha = k_\beta$) tends to the curve given by Case I (cigar type). For the present model, P is smaller than that of the TMK model; when $V_D \to \infty$, P approaches the value of the TMK model, and if Pe is smaller, it approaches that of the JH model.[5]

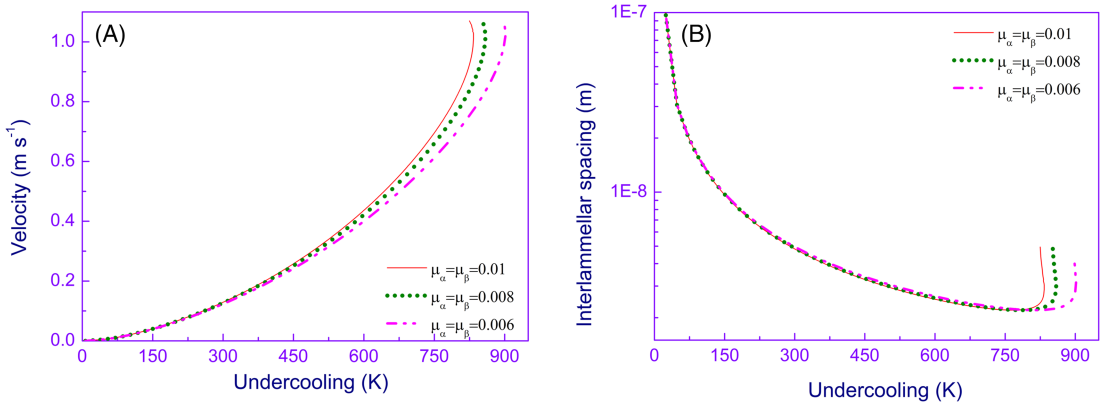

FIGURE 5 Effect of kinetic coefficient μ: (A) V-ΔT-V; (B) λ-ΔT [Colour figure can be viewed at wileyonlinelibrary.com]

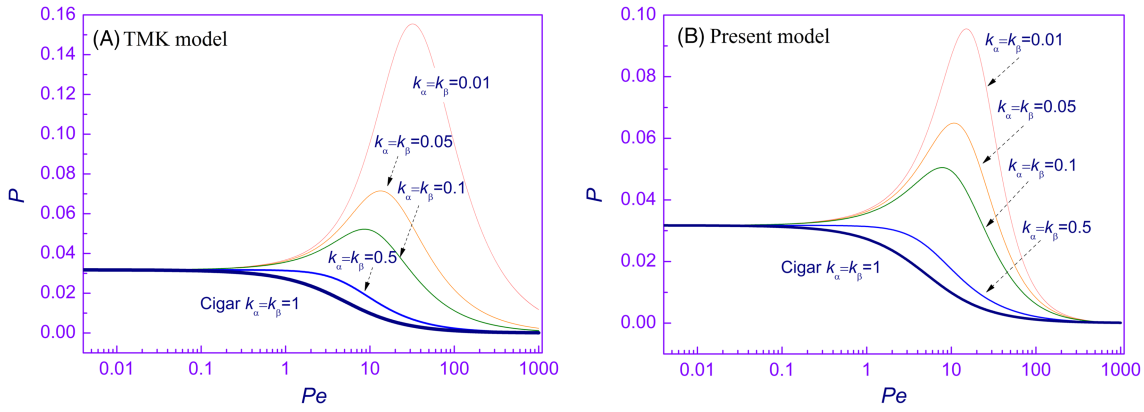

FIGURE 6 Function P in dependence of the Péclet number for $f = 0.4$, $k_\alpha = k_\beta = 0.01 \sim 1$: (A) function P of the TMK model; (B) function P of the present model [Colour figure can be viewed at wileyonlinelibrary.com]

3.7 | Effect of phase diagram

For cigar-type phase diagrams, generally k_α and k_β are not equal. For comparing the calculated results for Cases I (cigar) and II ($k_\alpha = k_\beta$) phase diagrams, we used the parameters as $C_{s\alpha}/C_{s\beta}/m_\alpha/m_\beta/C_E/T_e/V_D/k_\alpha/k_\beta/\mu$ = 0.002/0.998/450/450/0.5/1400/0.2/0.004/0.004/0.1, respectively, in Equations 4 and 9 to calculate the V-ΔT and λ-ΔT curves, as shown in Figure 7A,B, respectively. It is found that the V-ΔT curve for Case I is slightly higher than that for Case II, and the λ-ΔT curves almost coincide at all undercoolings. Generally, for Case II ($k_\alpha = k_\beta$), the solid solubility of the two eutectic phases is smaller and that for Case I (cigar) is larger, so Case II features a lower growth velocity than Case I, as expected. The result also indicates that relaxing the assumptions of small Péclet numbers has a stronger effect on the V-ΔT curve but only a small effect on the λ-ΔT curve. When $k \to 1$, the solidification interval becomes narrow, and Cases II and I tend to be the same.

3.8 | Effect of the concentration distribution at the interface

The plot of the solute concentration field $C(x,z)$ calculated by eq. (3a) in Xu and Galenko[9] with V = 7 and 14 mm s^{-1} is shown in Figure 8A,B, respectively. The parameters are $\Delta C_\alpha/\Delta C_\beta/m_\alpha/m_\beta/C_E/T_e/V_D$ = 0.48/0.48/450/450/0.5/1400/2, respectively. The plot shows how the solute concentration field changes periodically along lamellae but decreases in amplitude with distance away from the interface. With increasing V, the interface concentration $C(x,0)$ increases, and the periodic interval in x direction decreases. With faster growth velocity, the solute atoms in liquid enrich the concentration boundary layer at the interface in liquid.

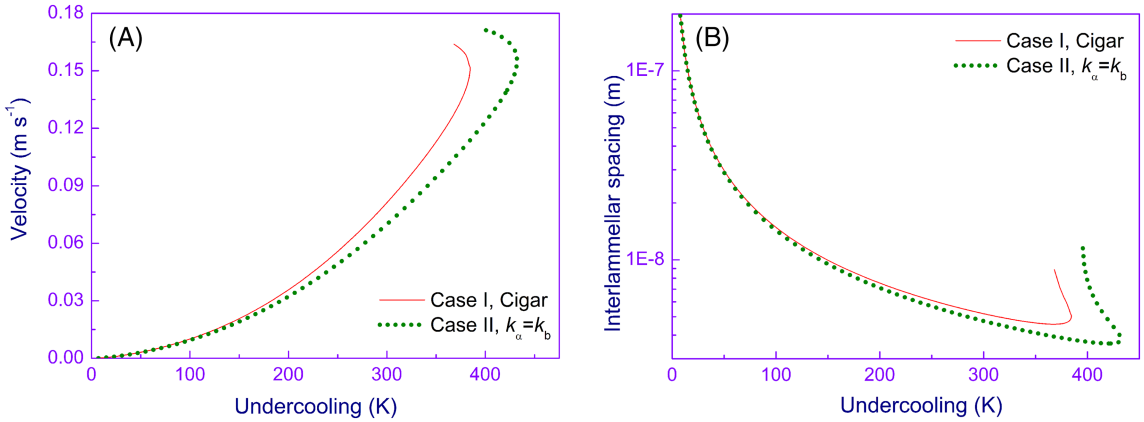

FIGURE 7 Calculations from diagram of Cases I (cigar) and II (equal k): (A) V-ΔT; (B) λ-ΔT [Colour figure can be viewed at wileyonlinelibrary.com]

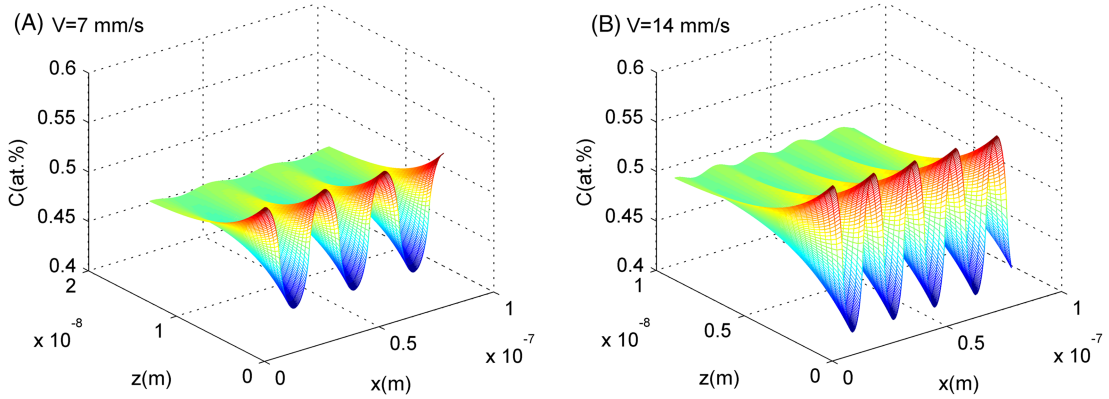

FIGURE 8 Plot of the solute concentration field for different growth velocities: (A) V = 7 mm s^{-1}; (B) V = 14 mm s^{-1} [Colour figure can be viewed at wileyonlinelibrary.com]

3.9 | Effects of further parameters on the V-ΔT and λ-ΔT curves

Besides the calculation with different parameters in Sections 3.2–3.7, the thermophysical parameters ΔH, C_p, and thermal diffusivity α also have an effect on the growth velocity. Particularly, with an increase of D, k, μ, V_D, C_p, and α and a decrease of m and ΔH, the velocity increases, and the undercooling decreases, as demonstrated in Figure 9.

4 | COMPARING MODEL RESULTS WITH EXPERIMENTAL DATA

As shown in Xu and Galenko,[9] for a calculation six-phase diagram parameters, particularly ΔC_α and ΔC_β, m_α and m_β, C_E, T_e must be known, and further entities can be deduced from them, particularly $C_{s\alpha}$ and $C_{s\beta}$, k_α and k_β, and $T_{m\alpha}$ and $T_{m\beta}$. To compare the calculations of the present model with experimental results, the undercooled rapid solidification of Fe-17at%B alloy melt was investigated. The master alloy was prepared by high-frequency induction melting. The melt undercooling was achieved by the melt-fluxing method.[13] Several heating and cooling cycles were carried out to homogenize the melt and achieve high undercoolings. Using a high-speed camera, the growth velocities for different undercoolings were measured; see Figure 10. Comparing the experimental data with the predictions of various models using the parameters from Table 1, it can be seen that all the models fit the data well at low undercoolings. However, at higher undercoolings, only the present model can fit the data well.

5 | DISCUSSION

Figure 11 demonstrates that for growth velocities $V < V_D$, the kinetic curve V-ΔT calculated with the present model changes continuously with the increase of the velocity V up to a maximum undercooling ΔT_2^*. When V approaches V_D,

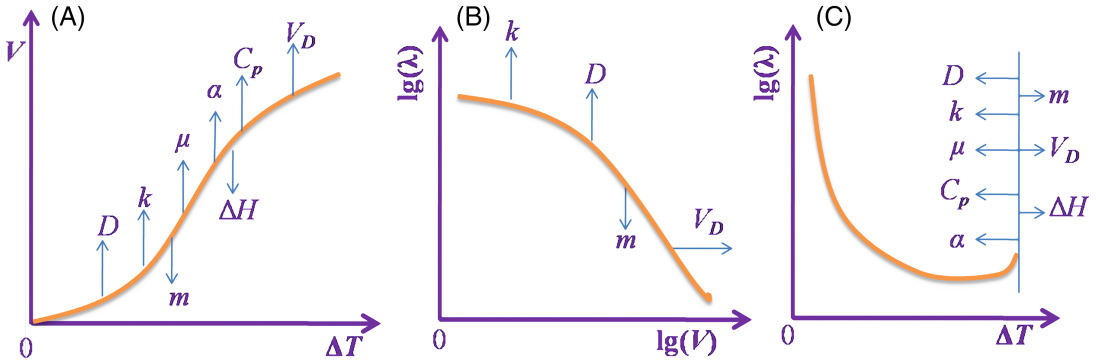

FIGURE 9 V-λ-ΔT curves affected by different parameters: (A) V-ΔT; (B) λ-V; (C) λ-ΔT [Colour figure can be viewed at wileyonlinelibrary.com]

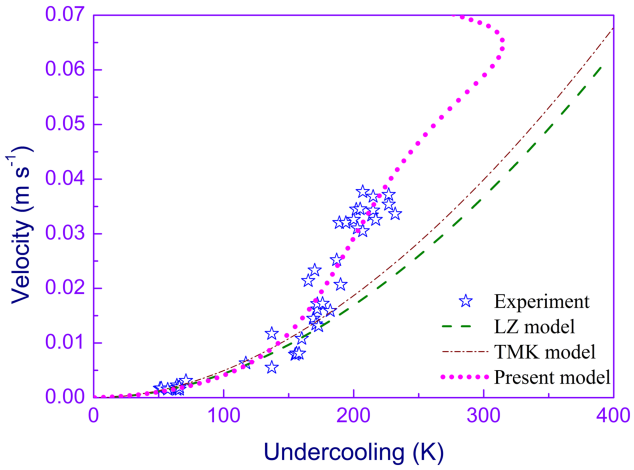

FIGURE 10 Theoretical predictions and experimental results for an Fe-17at%B eutectic alloy [Colour figure can be viewed at wileyonlinelibrary.com]

TABLE 1 The parameters for the model calculation of Fe/Fe_2B eutectic growth[13,14]

Parameter	Value	Parameter	Value
ΔH_α (J mol^{-1})	2.24×10^4	$C_{s\alpha}$	0.00017
ΔH_β (J mol^{-1})	1.38×10^4	$C_{s\beta}$	0.335
m_α (K at^{-1})	2030	T_e (K)	1454.4
m_β (K at^{-1})	1395	C_E (at)	0.17
V_D (m s^{-1})	0.09	α (m^2 s^{-1})	1.5×10^{-6}
C_P (J mol^{-1} K^{-1})	50	k_e	0.001
D_0 (m^2 s^{-1})	5×10^{-8}	E (J mol^{-1})	5×10^4

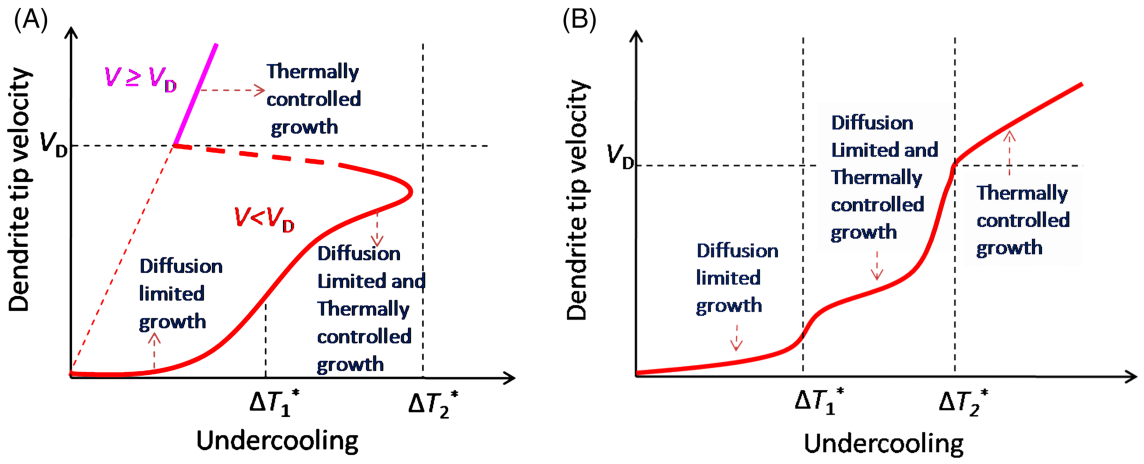

FIGURE 11 Schematic V-ΔT curves: (A) eutectic growth predicted by the present system of Equation 5; (B) dendritic growth as predicted by a sharp interface model in consistence with experimental data[12] [Colour figure can be viewed at wileyonlinelibrary.com]

growth may occur with a higher velocity at a lower undercooling. At the point $V = V_D$, the curve exhibits a discontinuity due to the ending of the diffusion-limited mode and the beginning of the diffusionless solidification. This mode proceeds further with $V > V_D$, with a suddenly reduced undercooling necessary for thermally controlled growth of the curved solid/liquid interface. This growth mode strongly differs from the dendrite growth kinetics in substitutional alloys. As shown in Figure 11B, the growth kinetics at the transition to purely thermally controlled growth in binary systems with $\Delta T = \Delta T_2^*$, the growth curve is continuous even though it has a break point. By contrast, the transition from diffusion-limited to purely thermally controlled growth in eutectic binary systems with $\Delta T = \Delta T_2^*$, the growth curve is discontinuous, Figure 11A. Experimental evidence for this regime is not available, but it should be observable in future natural or computational experiments.

We specially note that if the thermal undercooling is high enough in comparison with other contributions, the Ivantsov function, Iv, for a eutectic dendrite must be used in Equation 5. This means that at high undercoolings, the growth front features a dendrite tip shape (parabola-like tip shape[12]), but there are eutectic lamellae inside the dendrite, as is shown in Xu and Galenko[9] for the condition of very fine lamellae in comparison with the dendrite tip radius, that is, with $\lambda << R$. In the absence of thermal undercooling, the solidification interface can, as a whole, be considered as planar.

6 | SUMMARY

New expressions for solute distribution coefficients and slopes of liquidus lines are supplied in this study. The effects of different parameters on the growth velocity and lamellar spacing for given undercoolings are discussed. The growth velocity increases with the increase of the material parameters D, k, μ, V_D, and C_p, while it decreases with the increase of the other set of material parameters m and ΔH. The model predictions are compared with experimental data for a

solidifying eutectic Fe–B alloy. Computational results show that the model agrees well with experimental data especially for both low and high undercoolings.

ACKNOWLEDGEMENTS

This work was also financially supported by the German Science Foundation (DFG) GA1142/11-1, the Science and Technology Program of Shaanxi Province (No. 2016KJXX-87), and the Foundation of Shaanxi Provincial Department of Education (No. 18JS050). Open access funding enabled and organized by Projekt DEAL.

CONFLICT OF INTEREST

This work does not have any conflicts of interest.

AUTHOR CONTRIBUTION

Authors contributed equally to the content of the paper.

ORCID

Junfeng Xu https://orcid.org/0000-0003-4962-9355
Peter K. Galenko https://orcid.org/0000-0003-2941-7742

REFERENCES

1. Wang Z, Lin X, Cao Y, Liu F, Huang W. Formation of anomalous eutectic in Ni-Sn alloy by laser cladding. *Opt Laser Technol.* 2018;99:154-159. https://doi.org/10.1016/j.optlastec.2017.08.026
2. Zhang F, Lai C, Zhang J, Zhang Y, Zhou Q, Wang H. Anomalous eutectics in intermediately and highly undercooled Ni-29.8at.%Si eutectic alloy. *J Cryst Growth.* 2018;495:37-45. https://doi.org/10.1016/j.jcrysgro.2018.05.012
3. Xu J, Liu F, Zhang D. In situ observation of solidification of undercooled hypoeutectic Ni-Ni_3B alloy melt. *J Mater Res.* 2013;28(14):1891-1902. https://doi.org/10.1557/jmr.2013.165
4. Gusakova OV, Galenko PK, Shepelevich VG, Alexandrov DV, Rettenmayr M. Diffusionless (chemically partitionless) crystallization and subsequent decomposition of supersaturated solid solutions in Sn–Bi eutectic alloy. *Phil Trans R Soc A.* 2019;377(2143):20180204. https://doi.org/10.1098/rsta.2018.0204
5. Jackson KA, Hunt JD. Lamellar and rod eutectic growth. *TMS of AIME.* 1966;236:1129-1142. https://doi.org/10.1016/B978-0-08-092523-3.50040-X
6. Trivedi R, Magnin P, Kurz W. Theory of eutectic growth under rapid solidification conditions. *Acta Metall.* 1987;35(4):971-980. https://doi.org/10.1016/0001-6160(87)90176-3
7. Li JF, Zhou YH. Eutectic growth in bulk undercooled melts. *Acta Mater.* 2005;53(8):2351-2359. https://doi.org/10.1016/j.actamat.2005.01.042
8. Wei XX, Lin X, Xu W, Huang QS, Ferry M, Li JF, Zhou YH. Remelting-induced anomalous eutectic formation during solidification of deeply undercooled eutectic alloy melts. *Acta Mater.* 2015;95:44-56. https://doi.org/10.1016/j.actamat.2015.05.014
9. Xu J, Galenko PK. Effects of local nonequilibrium in rapid eutectic solidification—Part 1: statement of the problem and general solution. *Math Meth Appl Sci.* 2020. the present issue. https://doi.org/10.1002/mma.6960
10. Kurz W, Trivedi R. Eutectic growth under rapid solidification conditions. *Metall Trans.* 1991;22(12):3051-3057. https://doi.org/10.1007/BF02650266
11. Aziz M J, Boettinger WJ. On the transition from short-range diffusion-limited to collision-limited growth in alloy solidification. *Acta Metall Mater.* 1994;42(2):527–537. https://doi.org/10.1016/0956-7151(94)90507-X
12. Galenko P, Jou D. Rapid solidification as non-ergodic phenomenon. *Phys. Rep.* 2019;818:1-70. https://doi.org/10.1016/j.physrep.2019.06.002
13. Xu J, Jian Z, Dang B, Zhang D, Liu F. Solidification behavior and cooling curves for hypereutectic Fe-21at.PctB Alloy. *Metall Mater Trans. A.* 2017;48(4):1817-1826. https://doi.org/10.1007/s11661-016-3941-5
14. Kuang W, Karrasch C, Wang H, Liu F, Herlach DM. Eutectic dendrite growth in undercooled Fe83B17 alloy: experiments and modeling. *Scripta Mater.* 2015;105:34-37. https://doi.org/10.1016/j.scriptamat.2015.04.022

How to cite this article: Xu J, Rettenmayr M, Galenko PK. Effects of local nonequilibrium in rapid eutectic solidification—Part 2: Analysis of effects and comparison to experiment. *Math Meth Appl Sci.* 2021;1–12. https://doi.org/10.1002/mma.7004